Stability Analysis of Coiled Tape Springs

Antonio Pedivellano,* and Sergio Pellegrino†

California Institute of Technology, Pasadena, CA, 91125

Tape springs have been used for many years in deployable booms and space mechanisms and currently are being considered as components for more advanced deployable structures. Tape springs can be elastically coiled and will self-deploy when released. Their stability in the packaged configuration is critical for these applications. We propose a numerical and analytical framework to investigate the stability of coiled isotropic tape springs, where neither tension nor radial pressure are applied. Torsional and bending instabilities were observed when the ratio between the coiled radius and the radius of the cross-section exceeded a critical value. A stability boundary is derived for different geometries and material properties. The effect of varying the number of coils and the self-contact conditions between adjacent loops of a tape spring are also studied, as well as the existence of out-of-plane instability modes is discussed.

Nomenclature

R	=	radius of hub
r	=	radius of cross-section
b	=	arc-length of cross-section
α	=	angle subtended by cross-section
L	=	length of boom
u_i	=	displacement in i-th direction
ϕ_i	=	rotation about i-th axis
κ_{xx}	=	curvature in x-direction
κ_{yy}	=	curvature in y-direction
σ_{ij}	=	components of Cauchy stress tensor

I. Introduction

Large space structures need to be packaged to fit in a launch vehicle and to be deployed once in space. Coilable booms are widely used because they can be tightly wrapped around a cylindrical hub and are able to self-deploy by releasing stored strain energy from the packaging process.

There is a wide-ranging literature on the topic of deployable boom structures that investigates different cross-sections in order to obtain bistable behavior [1][2][3], ways to increase packaging efficiency [4], and mechanical properties in the deployed configuration [5].

One of the most common boom geometries is the tape spring, whose cross section consists of a circular arc of radius r. Due to their simplicity and cost-effectiveness, steel tape springs have been used for several CubeSat missions as UHF/VHF antennas [6] [7]. More advanced applications have used composite tape springs with embedded copper wires to achieve specific mechanical and electrical properties [8].

One of the main properties of tape springs is that there exists a natural radius of longitudinal curvature for which they are in equilibrium in the coiled configuration without any applied tension [9]. For isotropic tape springs, the natural radius of curvature corresponds to the radius of the cross section in the undeformed configuration. Whenever the tape spring needs to be coiled with a different radius of curvature, an external force must be applied to conform the tape spring to the desired geometry. Usually, this is done either by applying tension [10][11] or radial pressure [12].

---

*Graduate Student, Graduate Aerospace Laboratories, 1200 E California Blvd. MC 205-45. e-mail: `apedivel@caltech.edu`

†Joyce and Kent Kresa Professor of Aerospace and Civil Engineering, Graduate Aerospace Laboratories, 1200 E California Blvd. MC 105-50. AIAA Fellow. e-mail: `sergiop@caltech.edu`

In the absence of these constraints, several phenomena may occur, depending on the ratio R/r, between the coiling radius and the cross-section radius. When the ratio R/r is less than 1, the boom might undergo blossoming [12], leading to potential damage or jamming the deployment system. For larger values of R/r, the tape spring tends to form localized folds between straight segments [11].
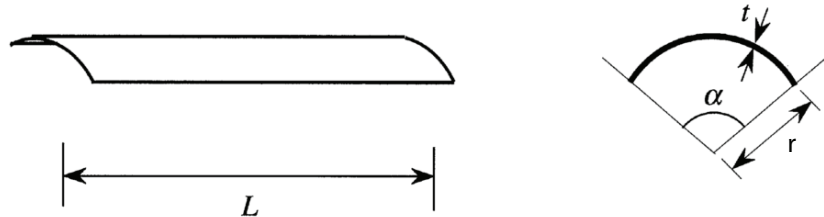
Fig. 1 Geometry of a tape spring (adapted from Seffen and Pellegrino[13])

A recent study quantified the minimum tension force required to prevent blossoming or localized folds on opposite-sense coiled tape springs [11]. One important result showed that the behavior of isotropic coiled tape springs could be classified in three regions: a bending-dominated region, for $R/r < 1$, a tension-dominated region for $R/r >> 1$ and an intermediate region, with more complex behavior. In this region, the tension required to keep the boom in the desired configuration is almost zero. Hence, this intermediate region is very desirable for practical applications, because it allows for simpler deployment mechanisms, in which neither tension nor radial constraints are required.

The objective of the present work is to analyze in more detail the range of R/r for which tension stabilization is not required in order to understand the limits of this region and to quantify the stability of equilibrium configurations. To that end, a computational framework was developed to study the stability of coiled tape springs, which we discuss in the rest of this paper.

The first section deals with the idealized case of an infinitely long tape spring with negligible thickness and perfect bonding between adjacent loops. Under these assumptions, it is possible to consider a single loop as representative of the stability of the entire structure. A numerical parametric study is performed to understand the effect of geometric and material properties on the stability behavior of the coiled tape spring.

Analytical models have been developed in the past to study bistable tape springs [1] [2] [14] [15], but these previous studies only considered uniform deformation modes. Instead, the numerical results from the present work suggest that non-uniform modes, with variable radius along the azimuthal direction, play a critical role and should be accounted for.

For this reason, we propose a new analytical model that combines an existing tape spring constitutive model [2] with standard energy methods [16] [17] to perform linear stability analyses about the initial uniformly-coiled configuration while accounting for non-uniform bending and torsional deformation modes.

At the end of this paper, we relax some of the initial assumptions to consider the effects of finite length and thickness. Finally, we allow relative motion between adjacent loops to assess its impact on the stability boundary.

II. Problem Statement

The objective of this paper is to study the stability of coiled tape springs when neither radial pressure nor tension are applied to conform them to the coiled radius. For such a geometry, the only necessary external action is a bending moment at the two ends of the boom, necessary to prevent self-deployment.

In particular, in this work we are interested in the limit of very long booms, for which $L >> R$, i.e. when the number of coils of the boom around the hub is large. Also, we assume that slipping between adjacent coils is prevented; this could be achieved by friction or by wrapping a string around the tape spring (Fig. 3(a)) . In the last section of this paper, we relax both assumptions and discuss their effects on the stability behavior of the tape spring.

Because of the no-slip condition between the coils, blossoming is prevented and the rotational symmetry of the tape spring is preserved. This allows to consider a "representative" element of the coiled structure, consisting of a single coil extracted from the inner region of the stowed boom (Fig. 3(b)).

Since the booms considered in this work are thin shells with $t << R$, the longitudinal radius of curvature changes slowly along the arc-length and can be considered constant for a single coil.

Therefore, a possible idealization for this problem is to consider a continuous ring with a given longitudinal radius
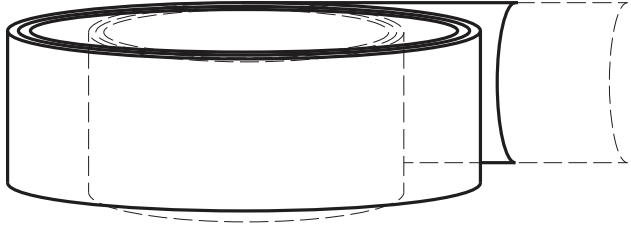
(a) Example of uniform buckling mode (blossoming): the dotted lines describe the initial configuration, the continuous lines the buckled one
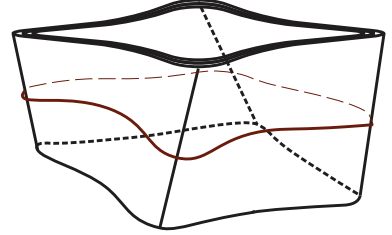

(b) Example of non-uniform buckling mode

Fig. 2 Problem formulation for the stability analysis of coiled tape springs. a) shows an uniform bending mode, known in literature as blossoming; b) shows a general non-uniform bending and twisting buckling mode. The red line describes the radial constraints preventing slipping between the coils.

of curvature R (Fig. 3(c)). Such a model offers two main advantages: from the computational standpoint, it facilitates the exclusion of edge effects that are not negligible when studying the global response of the structure; from the mathematical standpoint, it allows the use of periodic deformation modes to simplify the governing equations for the problem.
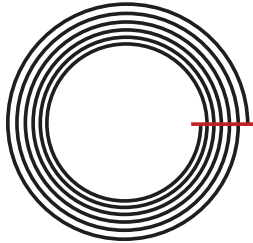
(a) Coiled tape spring
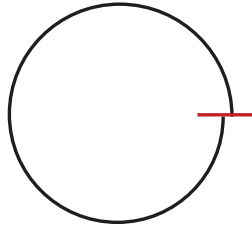
(b) Representative coil element
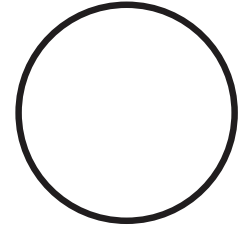
(c) Continuous ring

Fig. 3 Idealization process in the problem formulation: a) shows the fully coiled tape spring, where the red line indicates the no-slip constraint; b) extracts a representative coil from the full tape spring; c) connects the two ends of the representative element to obtain a continuous ring.

To simplify the number of parameters governing this problem, a linear elastic material was considered, and its effect was studied in terms of a single parameter, the Young's modulus E. A reference geometry for the cross-section in the deployed configuration was also picked by assigning a subtended angle $\alpha = 90°$, a transverse radius of curvature $r = 12.7$ mm and a thickness $t = 0.1$ mm. If not otherwise specified, the results shown in this paper are for steel tape springs with the geometry described above.

For a given geometry and material, the problem is controlled by a single parameter, the ratio R/r, which is commonly used in the literature to study the coiling of tape springs [12]. Since previous studies [11] have shown that the range of R/r for which a coiled tape spring does not require external tension is $1 \leq R/r \leq 3$, the present work explored configurations with $R/r > 0.75$ and studied the evolution of eigenvalues and eigenvectors as a function of this parameter, for different geometries, materials and coiling directions.

III. Numerical Model

We developed a finite element model in Simulia Abaqus using the previously described assumptions. The stability problem was solved in a two-step analysis, based on an implicit integration scheme. The first step generated the reference configuration of the tape spring with an assigned longitudinal radius of curvature; the exact shape of the cross section and its stress distribution were calculated. These results were then imported as initial conditions for the second step, in which a linear stability analysis was performed in order to extract eigenvalues and eigenvectors of the coiled tape spring.

One possible approach to model this problem is to coil an undeformed tape spring, with length $L = 2\pi R$, around a rigid hub of radius R and, subsequently, join the two ends of the tape spring in order to obtain a continuous ring.

The downside of such a modeling technique is that, due to numerical errors and edge effects, the stress distribution at the location where the two ends are connected would be different from the inner region. The first consequence is that the hypothesis of uniform stress distribution along the azimuthal direction of the ring is violated, so the results from the modal analysis would be affected by undesired edge effects. Additionally, such an approach would lead to in-plane stretching of the tape spring, unless the position of the neutral axis in the coiled configuration was known in advance and the length of the boom was adjusted accordingly.

An alternative strategy to overcome these challenges, which was implemented in this paper, is to coil only a portion of the tape spring, and extract the stress distribution and displacements across a representative section in the uniformly coiled region. Then, these values can be used to define the shape and stress distribution of each cross section of a second model that consists of a coiled tape spring forming a full ring. In this way, by construction, any edge effect is effectively removed from the model, achieving the state of uniform coiling desired as the starting point for the stability analysis.

In the following sections, the solution strategies are discussed in more detail and the results are presented.

A. Coiling

The objective of this analysis is to achieve a stretching-free, uniformly coiled tape spring. To this extent, a partial model was built by using only 1/4 of a turn around a circular hub and using the symmetries of the model (as shown in Fig. 4).
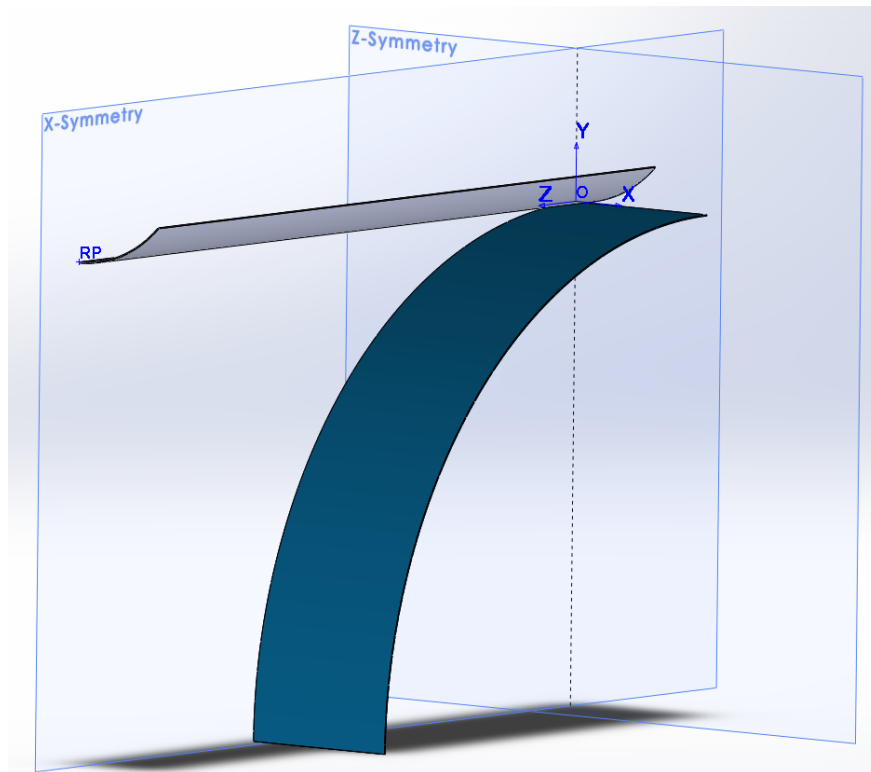
Fig. 4   Partial model for a tape spring (in grey) coiled around a rigid cylindrical hub (in blue) for a coiling ratio $R/r = 4$

The boundary conditions were chosen in such a way as to be compatible with the hypothesis of uniform coiling, allowing for free deformation of the cross-section of the tape spring. At $z = 0$, this was achieved by using symmetric boundary conditions with respect to the z-axis, corresponding to $u_z = 0$, $\phi_y = 0$, $\phi_x = 0$, where u_i are displacements along the i-th axis and ϕ_i are rotations about the i-th axis. Therefore, a mirror image of the solution with respect to the plane $z = 0$ was formed.

Since only a quarter of a turn of the coiled tape spring was modeled, a possible way of defining the boundary condition at the opposite end, $z = L$, was by applying a transverse displacement $u_y = -R$. In order to allow for changes of the cross-section shape at this location, the displacement boundary condition was applied only to a reference point,

lying on the mid-line (labeled RP in Fig. 4).

The remaining points of the cross-section were constrained to lie on a plane normal to the mid-line. This was achieved by creating a local coordinate system attached to the cross section at $z = L$ and defining an equation constraint such that $\tilde{u}_z^i - \tilde{u}_z^0 = 0$, where "0" refers to the reference point, whereas "i" refers to the remaining points on the cross section and $\tilde{u}_z$ describes the z-displacements in the local frame.

This additional boundary condition accomplished two objectives:

- distributing the tip load across the whole section, thus preventing stress / strain singularities due to the displacement boundary condition applied to a single point;
- preventing in-plane shear at the tip of the boom, which would be incompatible with the hypothesis of uniform coiling.

In order to obtain accurate static results without significantly increasing the computational cost of the analysis, an implicit integration scheme was used. However, using a static implicit solver for this highly non-linear problem, characterized by shell contacts and snap-through instabilities, would have made convergence of the solver difficult to achieve. Therefore, we chose an alternative approach, consisting of a dynamic implicit step, where numerical damping is used in order to obtain a quasi-static solution [18]. This combines the robustness of a dynamic formulation with the unconditional stability of implicit solvers. The resulting stress distribution is shown in Fig. 5.


(a) Longitudinal stress

(b) Transverse stress
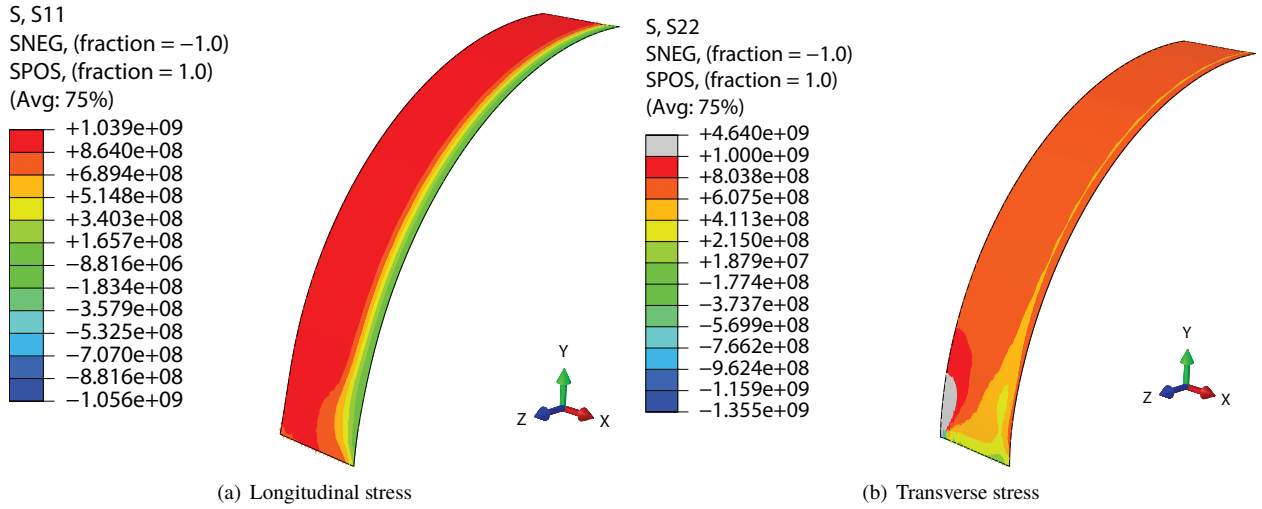
Fig. 5 Stress distribution in the tape spring at the end of the partial coiling process (the hub is not shown) for a ratio $R/r = 3$. S_{11} and S_{22} are the stresses (in Pa) along the longitudinal and transverse direction, expressed in the material frame. The values plotted correspond to the top surface of the shell.

It can be observed that the stress is uniform in most of the tape spring, except for a small region near the ends. Therefore, the representative cross-section was chosen in the uniform region. For the case $R/r = 3$, the resulting stress components are plotted in Fig. 6.

Having used S4R elements for computational efficiency, each element only contained a single integration point and 5 section points across the thickness. The element formulation assumes linear strain variation in the direction normal to the shell and therefore, for an isotropic material, the values of the stress at the top and bottom section points of the element are sufficient to fully characterize its stress distribution. For this reason, the plots in Fig. 6 show the stress distribution along the cross-section (described by a normalized transverse coordinate) for the top and bottom section point.

To verify the assumptions of stretching-free coiling, the numerical stress distribution was compared with a simplified analytical model that consists of a thin plate subjected to pure bending in two directions. In the undeformed configuration, the natural curvature vector for opposite sense coiling is:

$$\boldsymbol{\kappa}^0 = \begin{bmatrix} \kappa_{xx}^0 \\ \kappa_{yy}^0 \\ \kappa_{xy}^0 \end{bmatrix} = \begin{bmatrix} 0 \\ -\frac{1}{r} \\ 0 \end{bmatrix} \tag{1}$$

5
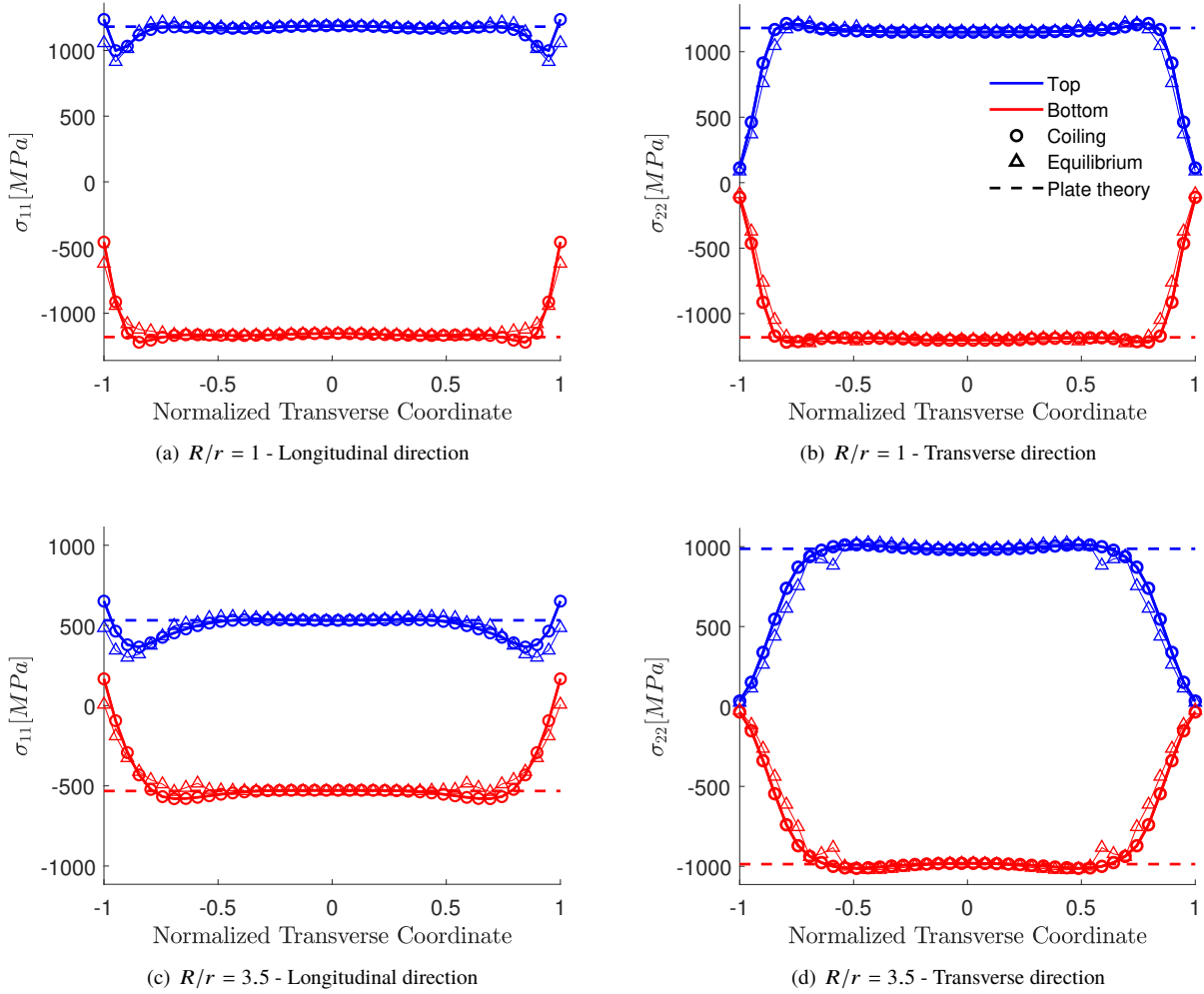
Fig. 6 Stress distribution along the cross-section of an opposite-sense coiled tape spring for different ratios R/r. The blue and red curves describe, respectively, the stress on the top and bottom face of the shell. The dashed lines are the predicted stresses from plate theory, the circles are the FE results from the coiled model and the triangles are the FE results after removing the hub.

where x and y are the longitudinal and transverse direction, respectively. For opposite sense coiling, a first-order approximation for the curvature is:

$$\boldsymbol{\kappa}^1 = \begin{bmatrix} \kappa_{xx}^1 \\ \kappa_{yy}^1 \\ \kappa_{xy}^1 \end{bmatrix} = \begin{bmatrix} \frac{1}{R} \\ 0 \\ 0 \end{bmatrix} \tag{2}$$

which corresponds to the assumption of perfect flattening of the cross-section. In reality, this approximation only holds in the inner region, not at the edges, where a bending moment would need to be applied to the free edge.

Therefore, the change in curvature during the coiling process is:

$$\Delta \kappa_x = \kappa_x^1 - \kappa_x^0 = -\frac{1}{R} \tag{3a}$$

$$\Delta \kappa_y = \kappa_y^1 - \kappa_y^0 = \frac{1}{r} \tag{3b}$$

6

From Kirchhoff-Love plate theory, the strain distribution is as follows:

$$\epsilon_{xx} = \epsilon^0_{xx} + z\Delta\kappa_{xx} = -\frac{z}{R} \tag{4}$$

$$\epsilon_{yy} = \epsilon^0_{yy} + z\Delta\kappa_{yy} = \frac{z}{r} \tag{5}$$

$$\epsilon_{xx} = \epsilon^0_{xy} + 2z\Delta\kappa_{xy} = 0 \tag{6}$$

where ϵ^0_{xx}, ϵ^0_{yy} and ϵ^0_{xy} are the in-plane strains of the mid-plane, identically zero for pure bending. Using the constitutive model for an isotropic material, the stresses are given by:

$$\sigma = \frac{E}{1-v^2}\begin{bmatrix} 1 & v & 0 \\ v & 1 & 0 \\ 0 & 0 & \frac{1-v}{2} \end{bmatrix}\begin{bmatrix} \epsilon_{xx} \\ \epsilon_{yy} \\ \epsilon_{xy} \end{bmatrix} = \frac{E}{1-v^2}\begin{bmatrix} -\frac{z}{R} + v\frac{z}{r} \\ -v\frac{z}{R} + \frac{z}{r} \\ 0 \end{bmatrix} \tag{7}$$

Therefore, the stresses are symmetric with respect to the mid-surface of the shell. Fig. 6 compares this simple model with the numerical results and shows very good agreement in the inner region of the cross-section. This confirms that the boom is actually subjected to pure bending. Also, Fig. 6 shows that the outer region of the cross-section deviates from plate theory due to edge effects, which cannot be captured by the uniform kinematic model of Eq.3. In this region, the presence of a free edge requires that $\sigma_{22} = 0$, and its gradient is balanced by in-plane shear stresses σ_{12}, which in turn affect the distribution of longitudinal stress σ_{11}.

B. Stability

In order to obtain the coiled configuration of the tape spring, a new model was generated by rotating the deformed cross-section extracted from the previous analysis about a central axis. This provided the initial geometry for the stability analysis, uniform in the azimuthal direction by construction while accounting for the actual coiled cross-section.

Additionally, the prestress derived from the coiling process was included by using the Abaqus subroutine SIGINI [18], which assigns a stress tensor to each section point of each element in the model at the beginning of the analysis.
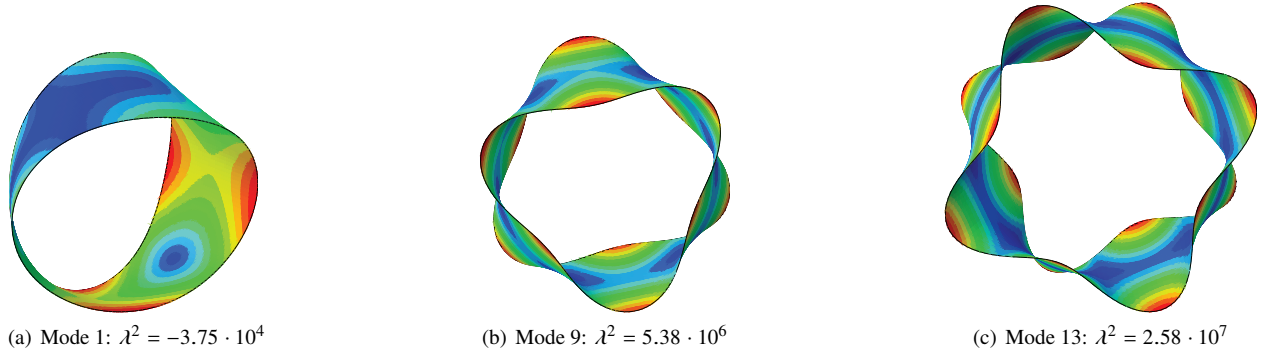
Note that, in this case, the hub was not included in the model, since the objective of the study was to assess the stability of the coiled tape spring when no radial constraints were applied. Therefore, the first part of the analysis consisted of a static equilibrium step, in order to allow possible stress redistribution due to the modified boundary conditions. The resulting stress components along the cross-section are shown in Fig. 6. It can be observed that some small adjustment occurred near the edges, but it did not change the overall distribution.

Finally, a linear stability analysis of the tape spring was performed near this coiled reference configuration and the first 100 eigenmodes were extracted. Repeating this process for several values of the parameter R/r, it was observed that the resulting eigenmodes could be classified in two main types: bending modes and twisting modes. Representative mode shapes for the two classes are shown in Figs. 7 and 8.


(a) Mode 5: $\lambda^2 = 3.64 \cdot 10^5$ (b) Mode 8: $\lambda^2 = 4.76 \cdot 10^6$ (c) Mode 15: $\lambda^2 = 3.06 \cdot 10^7$
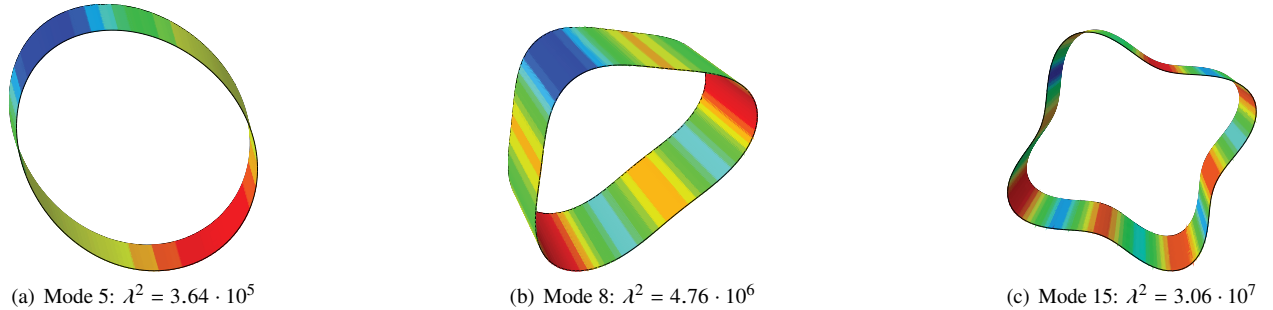
Fig. 7   Example of bending modes for a coiled tape spring with $R/r = 1.9$.

Fig. 9 contains the lowest eigenvalues for the reference geometry ($\alpha = 90°$, $t = 0.1$ mm and $E = 270$ GPa) when coiled with different ratios R/r. Starting from large positive values for small ratios R/r, the smallest eigenvalue monotonically decreases until it becomes negative, marking the limit of the stable region. The two lines in the plot correspond to equal and opposite sense coiling and show that the former has a significantly lower stability limit, with a critical value of $(R/r)_{cr} = 1.54$, whereas the latter becomes unstable for $(R/r)_{cr} = 7.7$.

7

(a) Mode 1: $\lambda^2 = -3.75 \cdot 10^4$ (b) Mode 9: $\lambda^2 = 5.38 \cdot 10^6$ (c) Mode 13: $\lambda^2 = 2.58 \cdot 10^7$

Fig. 8   Example of torsional modes for a coiled tape spring with $R/r = 1.9$.
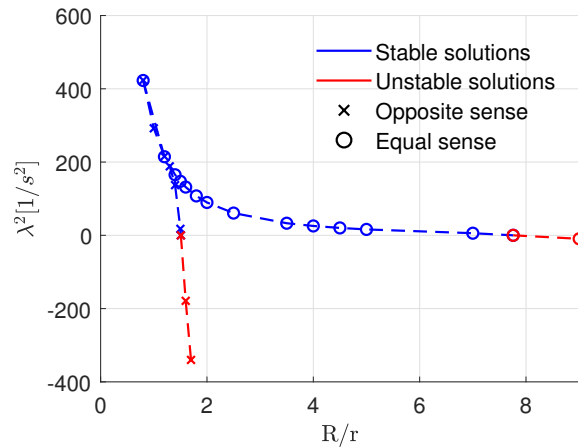
Fig. 9   Lowest eigenvalues of the coiled reference geometry, as a function of the ratio R/r for equal and opposite sense coiling.

It is interesting to note that, for opposite sense coiling, the instability is triggered by torsional modes, whereas for equal sense coiling the first negative eigenvalue corresponds to a bending mode. In both cases, once the stability limit is crossed, an infinite number of unstable modes appears, with varying wavenumber. This suggests that the stability boundary is unique for a given geometry and material, and does not depend on the specific mode considered. Later in the paper, this statement will be supported by the results obtained by an analytical formulation of the stability problem.

IV. Parametric study

Using the numerical model described in Sec. III, a parametric study was performed to study the effect of geometry and material properties on the stability of coiled tape springs. Starting from the reference geometry previously used, several values of thickness, subtended angle and Young's modulus were analyzed and the corresponding critical ratios R/r were determined. The objective was to define stability boundaries for each variable, so that stable and unstable regions could be identified in the tape spring design space.

Fig. 10 shows the effect of varying the angle subtended by the cross-section, for equal and opposite sense bending. In both cases, it can be seen that increasing the angle has a stabilizing effect on the coiled tape spring, since the critical ratio of R/r linearly increases with it. Note that the linear fit shown in red only holds for $\alpha > 0$. When $\alpha = 0$, i.e. when the tape spring degenerates in a flat strip, its tangent torsional stiffness drops to zero for any coiling radius and $(R/r)_{cr}$ becomes zero because $r \to \infty$.

The effect of varying the thickness is shown in Fig. 12. A cubic polynomial provides a good approximation of the distribution of the critical ratios of R/r as a function of non-dimensionalized thickness. The distribution reaches a minimum for relatively thin shells and increases for thicker tape springs.
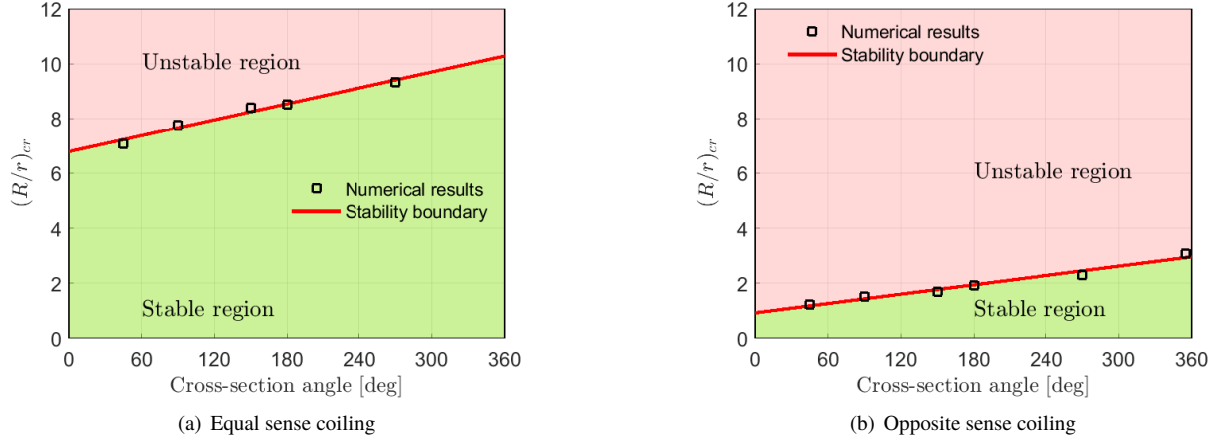
(a) Equal sense coiling

(b) Opposite sense coiling

Fig. 10 Stability boundary for coiled tape springs as a function of the angle subtended by the cross-section, assumed of fixed width

(a) Equal sense coiling

(b) Opposite sense coiling
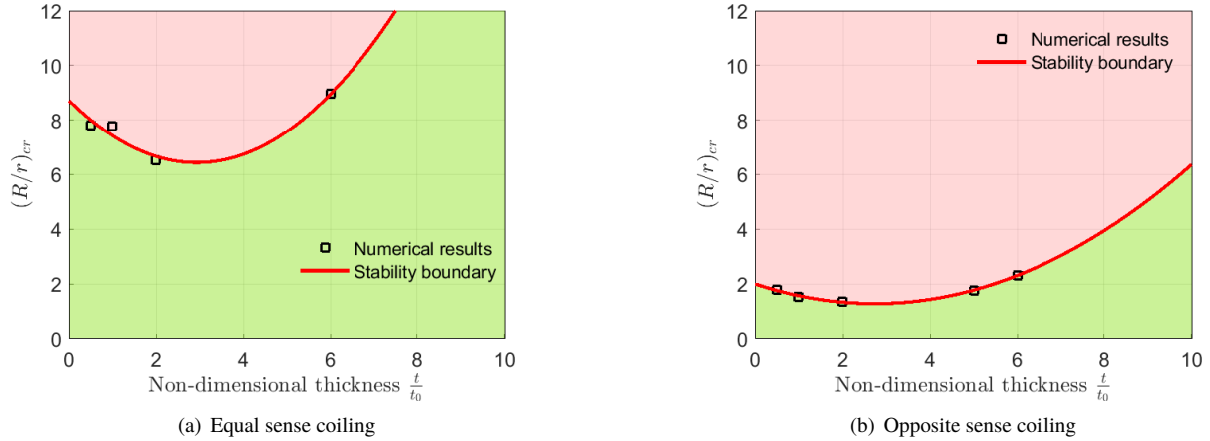
Fig. 11 Stability boundary for coiled tape springs as a function of the shell thickness. The values are non-dimensionalized by using a reference thickness $t_0 = 0.1$ mm.

V. Analytical Model

In this section, an analytical formulation of the stability problem for coiled tape springs is derived. The objective is to obtain a better understanding of the parameters governing the stability behavior and derive a quick design tool for assessing the stability of different systems. The formulation is based on the idealized problem of a closed-loop that neglects edge effects in the reference uniform configuration,as described in Fig. 3(c). Unlike the simple plate formulation used in Sec. III.A, in this section a more refined shell model will be used.

The kinematic model used in the following is based on classical shell theory [19] and includes the extra terms proposed by Galletly and Guest [2] to describe the uniform twisting of slit tubes with a circular arc cross-section.

The model first computes the reference coiled configuration by applying two uniform changes of curvature along the $x-$ and $y-$ direction. The equations of equilibrium for the shell are then written for the coiled geometry to compute the actual geometry of the cross-section such that the boundary conditions are satisfied. This geometry is described by an out-of-plane displacement w, corresponding to the deviation from the uniform reference configuration.

A one-dimensional constitutive model for the tape spring is derived using the principle of virtual work, and the pre-stress in the reference configuration is computed. Then, infinitesimal non-uniform perturbations to the equilibrium configuration are applied and the tangent stiffness matrix is derived. Finally, its eigenvalues are used to assess the stability of the equilibrium.

(a) Equal sense coiling
(b) Opposite sense coiling
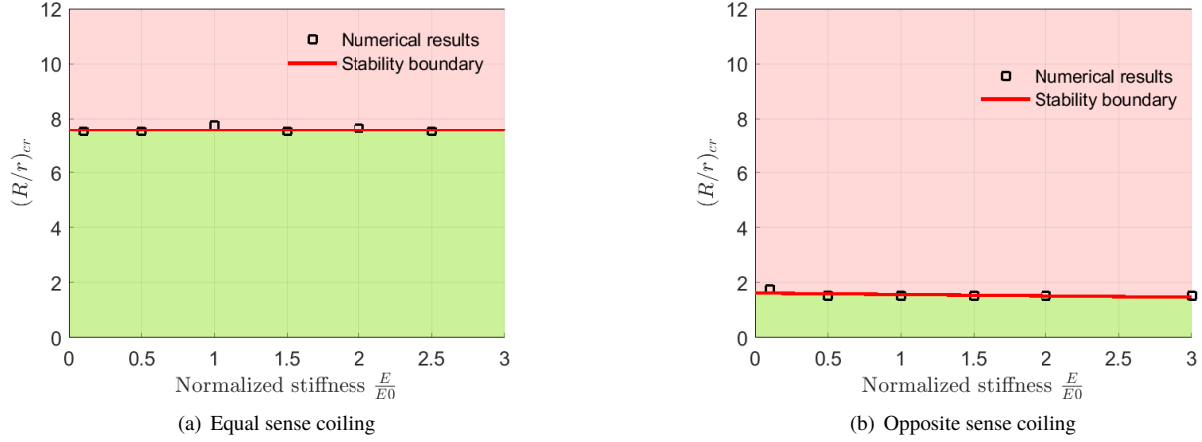
Fig. 12 Stability boundary for coiled tape springs as a function of Young's modulus. The values are non-dimensionalized by using a reference Young's modulus E_0 = 210 GPa.

A. Governing equations

The general kinematic equations for this problem are as follows:

$$\epsilon_x = Kw + \frac{\phi^2}{2}\left(y^2 - \frac{b^2}{12}\right) \tag{8a}$$

$$\kappa_x = K - \left[wK^2\right] - \frac{\partial^2 w}{\partial x^2} \tag{8b}$$

$$\kappa_y = \pm\frac{1}{r} - \frac{\partial^2 w}{\partial y^2} \tag{8c}$$

$$\kappa_{xy} = -2\phi \tag{8d}$$

where the sign of the first term on the right hand side of Eq. 8c depends on the coiling direction (positive for opposite sense, negative for equal sense). The model is defined in terms of two global kinematic variables: the twist of the cross-section ϕ and the curvature K (corresponding to the inverse of the hub radius). Note that, when the displacement w is small, the term in square brackets in Eq. 8c can be neglected.

It can be shown [19] that the equilibrium equations for a cylindrical shell when no external loads are applied can be combined in the following governing equation:

$$\frac{\partial^2 M_x}{\partial \kappa^2} + 2\frac{\partial^2 M_{xy}}{\partial x \partial y} + \frac{\partial^2 M_y}{\partial y^2} = KN_x \tag{9}$$

One of the assumptions made by Galletly and Guest [1] and accepted in this derivation is that $N_y = N_{xy} = 0$. This is identically true on the edges, where there is no external load applied, but the condition is assumed to be approximately satisfied everywhere. Therefore, ϵ_{yy} and ϵ_{xy} can be written in terms of the remaining strain variables and solved afterwards. This leads to a reduced order constitutive relation that, for an isotropic material, can be expressed as follows:

$$\begin{bmatrix} N_{xx} \\ M_{xx} \\ M_{yy} \\ M_{xy} \end{bmatrix} = \begin{bmatrix} A_{11}^* & 0 & 0 & 0 \\ 0 & D_{11} & D_{12} & 0 \\ 0 & D_{12} & D_{11} & 0 \\ 0 & 0 & 0 & D_{33} \end{bmatrix} \begin{bmatrix} \epsilon_{xx} \\ \kappa_{xx} \\ \kappa_{yy} \\ \kappa_{xy} \end{bmatrix} \tag{10}$$

where A_{11}^* is the reduced axial stiffness, given by:

$$A_{11}^* = A_{11} - \frac{A_{12}^2}{A_{11}} = Et \tag{11}$$

10

Combining Eq. 10 and Eq. 8 into Eq. 9, the governing equation can be written in terms of the displacement w and the two global deformations K and ϕ, to obtain:

$$\frac{\partial^4 w}{\partial x^4} + 2\nu \frac{\partial^4 w}{\partial^2 x \partial^2 y} + \frac{\partial^4 w}{\partial y^4} + \frac{AK^2}{D} w = -\frac{KA}{D} \left[\frac{\phi^2}{2} \left(y^2 - \frac{b^2}{12} \right) \right] \tag{12}$$

This is a linear fourth-order partial differential equation in $w(x, y)$ with non-constant coefficients due to the function $K(x)$. Since a closed-form solution does not exist, it was necessary to introduce an additional hypothesis, i.e. that the shape of the cross-section does not depend on the longitudinal coordinate, so that $w = w(y)$. Physically, this implies that cross-section at any location is only a function of the local longitudinal curvature and twist, without being affected by the adjacent portions of the tape spring. This assumption is reasonable when the global variables $K(x)$ and $\phi(x)$ vary over a characteristic length that is much larger than the dimension of the cross-section. As a consequence of this assumption, the governing equation reduces to an ordinary differential equation in y, which can be written as:

$$\frac{d^4 w}{dy^4} + \frac{4}{\mu^4} w = -\frac{4}{K\mu^4} \left[\frac{\phi^2}{2} \left(y^2 - \frac{b^2}{12} \right) \right] \tag{13}$$

with

$$\mu = \sqrt{\frac{2t}{K\sqrt{12(1 - \nu^2)}}} \tag{14}$$

The general form of the solution to this equation has the expression:

$$w(y) = c_1 \sin \frac{y}{\mu} \sinh \frac{y}{\mu} + c_2 \cos \frac{y}{\mu} \sinh \frac{y}{\mu} + c_3 \sin \frac{y}{\mu} \cosh \frac{y}{\mu} + c_4 \cos \frac{y}{\mu} \cosh \frac{y}{\mu} - \frac{\Phi^2}{2K} \left(y^2 - \frac{b^2}{12} \right) \tag{15}$$

where c_1, c_2, c_3 and c_4 are integration constants calculated from the boundary conditions.

Regardless of the coiling direction, the boundary conditions for Eq. 15 are the same when the tape spring has no contact with the hub. In this case, both bending moment and shear force on the edges of the cross-section must be zero, so the following conditions are valid:

$$Q_y \left(\pm \frac{b}{2} \right) = \left. \frac{dM_y}{dy} \right|_{y=\pm\frac{b}{2}} = 0 \tag{16a}$$

$$M_y \left(\pm \frac{b}{2} \right) = 0 \tag{16b}$$

The following solution to Eq. 15 with these boundary conditions was derived in [2], in the context of bistable slit tubes:

$$w(y) = -\frac{\mu^2}{2} \left[\pm \frac{1}{r} - \frac{\phi^2}{K} - \nu K \right] \left[c_1 \sin \frac{y}{\mu} \sinh \frac{y}{\mu} + c_4 \cos \frac{y}{\mu} \cosh \frac{y}{\mu} \right] - \frac{\Phi^2}{2K} \left(y^2 - \frac{b^2}{12} \right) \tag{17}$$

where:

$$c_1 = \frac{\sinh \frac{b}{2\mu} \cos \frac{b}{2\mu} + \cosh \frac{b}{2\mu} \sin \frac{b}{2\mu}}{\sinh \frac{b}{2\mu} \cosh \frac{b}{2\mu} + \sin \frac{b}{2\mu} \cos \frac{b}{2\mu}} \tag{18a}$$

$$c_4 = \frac{\sinh \frac{b}{2\mu} \cos \frac{b}{2\mu} - \cosh \frac{b}{2\mu} \sin \frac{b}{2\mu}}{\sinh \frac{b}{2\mu} \cosh \frac{b}{2\mu} + \sin \frac{b}{2\mu} \cos \frac{b}{2\mu}} \tag{18b}$$

and the sign of the first term in square brackets depends of the coiling direction (positive for equal sense, negative for opposite sense coiling).

Fig. 13 compares the result from Eq. 17 with the cross-sectional shape extracted from the finite element model in opposite sense coiling. The results show a good agreement, predicting a central flat region, with a small oscillation near the edges of the shell, whose amplitude increases with the coiling radius.

(a) $R/r = 1$ (b) $R/r = 6$
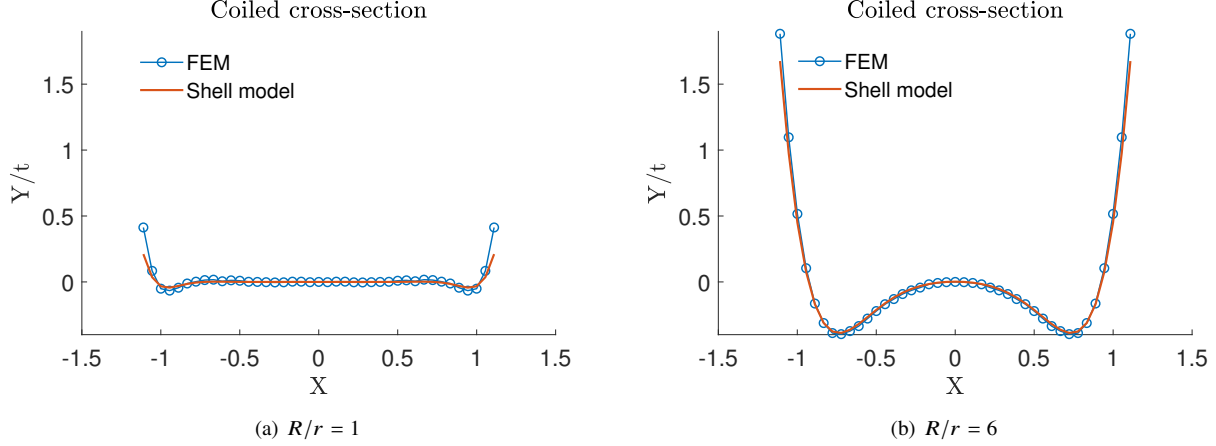
Fig. 13 **Comparison between the cross-sectional shape of an opposite-sense coiled tape spring from the numerical model and the analytical prediction, for different radii ratios. The X-axis contains the normalized arc-length of the cross-section, whereas the Y-axis describes the shape of the cross-section (not to scale), as a percentage of the shell thickness.**

B. One-dimensional Constitutive Model

A standard approach used when studying tape springs is to develop 1-D constitutive models by defining global kinematic variables and computing the corresponding global forces by using the principle of virtual work. For the shell model used in this formulation, the global kinematics are described by the longitudinal curvature K and the twisting ϕ, whose energy-conjugate global forces are the bending moment M and the twisting moment T.

Using the constitutive model from Eq. 10, M and T can be computed as follows:

$$M = \int_0^L \left(M_{xx} \frac{\partial \kappa_{xx}}{\partial K} + M_{yy} \frac{\partial \kappa_{yy}}{\partial K} + M_{xy} \frac{\partial \kappa_{xy}}{\partial K} + N_x \frac{\partial \epsilon_{xx}}{\partial K} \right) dy \tag{19a}$$

$$T = \int_0^L \left(M_{xx} \frac{\partial \kappa_{xx}}{\partial \Phi} + M_{yy} \frac{\partial \kappa_{yy}}{\partial \Phi} + M_{xy} \frac{\partial \kappa_{xy}}{\partial \Phi} + N_x \frac{\partial \epsilon_{xx}}{\partial \Phi} \right) dy \tag{19b}$$

Substituting the kinematics from Eq. 8 and the cross-sectional shape from Eq. 17 (with the appropriate signs depending on the coiling direction), a 1-D constitutive model can be obtained. The following result is adapted from Galletly and Guest [2]:

$$M = -Db \left\{ \frac{1}{K} \left[\frac{\Phi^2}{K} + \nu K \pm \frac{1}{r} \right]^2 d_2 + \left[\frac{\Phi^2}{K} + \nu K \pm \frac{1}{r} \right] \left[\frac{\Phi^2}{K^2} - \nu \right] d_1 - (1 - \nu^2)K \right\} \tag{20a}$$

$$T = 2Db \left\{ \left[\frac{\Phi^2}{K} + \nu K \pm \frac{1}{r} \right] \frac{\Phi}{K} d_1 + (1 - \nu)\Phi \right\} \tag{20b}$$

where d_1 and d_2 are given by:

$$d_1 = 1 - \frac{2\mu}{b} \left(\frac{\cosh \frac{b}{\mu} - \cos \frac{b}{\mu}}{\sinh \frac{b}{\mu} + \sin \frac{b}{\mu}} \right) \tag{21a}$$

$$d_2 = \frac{\sinh \frac{b}{\mu} \sin \frac{b}{\mu}}{\left(\sinh \frac{b}{\mu} + \sin \frac{b}{\mu} \right)^2} - \frac{\mu}{2b} \left(\frac{\cosh \frac{b}{\mu} - \cos \frac{b}{\mu}}{\sinh \frac{b}{\mu} + \sin \frac{b}{\mu}} \right) \tag{21b}$$

C. Stability Analysis

In this section, the stability of a tape spring about its uniformly coiled configuration is studied by computing the global tangent stiffness matrix C and considering the sign of its eigenvalues. To derive this matrix, we first consider an

adjacent equilibrium configuration, such that:

$$K = K_0 + K_1 \tag{22a}$$

$$\Phi = \Phi_1 \tag{22b}$$

where K_0 is the longitudinal curvature of the reference uniform configuration. Since no external load is applied, the total potential energy of perturbed configuration is:

$$\delta\Pi = \int_0^L (MK + T\Phi)dx = \int_0^L [(M_0 + M_1)(K_0 + K_1) + T_1\Phi_1]dx \tag{23}$$

where the subscripts "0" corresponds to the reference configuration and "1" to the perturbation.

Since the geometry consists of a closed loop, kinematic compatibility requires periodic mode shapes, so the following form of the perturbation is considered:

$$K_1 = -\left(\frac{2\pi n}{L}\right)^2 \bar{K}_1 \cos\frac{2\pi nx}{L} \tag{24a}$$

$$\Phi_1 = -\left(\frac{2\pi n}{L}\right) \bar{\Phi}_1 \sin\frac{2\pi nx}{L} \tag{24b}$$

$$\tag{24c}$$

where $\bar{K}_1$ and $\bar{\Phi}_1$ are the small amplitudes of the perturbations, whereas n is the integer wavenumber of the deformation.

This formulation is compatible with a displacement field of the form:

$$w = \bar{w}_0(y)\cos\frac{2\pi nx}{L} \tag{25}$$

since the curvature and the twist are related to the second and first derivative of w, respectively.

By expanding Eq. 23 to the second order with respect to the amplitudes $\bar{K}_1$ and $\bar{\phi}_1$, the following expression holds:

$$\delta\Pi = \delta\Pi|_{K_1=0,\phi_1=0} + \nabla\delta\Pi|_{\bar{K}_1=0,\bar{\phi}_1=0}\begin{bmatrix}\bar{K}_1\\\bar{\phi}_1\end{bmatrix} + \frac{1}{2}\begin{bmatrix}\bar{K}_1 & \bar{\phi}_1\end{bmatrix}H|_{\bar{K}_1=0,\bar{\phi}_1=0}\begin{bmatrix}\bar{K}_1\\\bar{\phi}_1\end{bmatrix} \tag{26}$$

where $\nabla\delta\Pi|_{\bar{K}_1=0,\bar{\phi}_1=0}$ is the gradient of the potential energy and $H|_{\bar{K}_1=0,\bar{\phi}_1=0}$ is the 2×2 Hessian matrix, corresponding in this case to the tangent stiffness matrix C:

$$C = \begin{bmatrix}\frac{\partial^2\delta\Pi}{\partial K_1^2} & \frac{\partial^2\delta\Pi}{\partial K_1\partial\phi_1}\\[2mm]\frac{\partial^2\delta\Pi}{\partial K_1\partial\phi_1} & \frac{\partial^2\delta\Pi}{\partial\phi_1^2}\end{bmatrix} \tag{27}$$

Substituting the kinematics for the adjacent equilibrium configuration (Eq. 22) in the global constitutive relations (Eq. 20), the perturbed potential energy can be written in terms of the perturbations K_1 and ϕ_1. Because of the non-linearity of the constitutive model, some approximation is necessary to obtain a closed-form expression for the tangent stiffness matrix. To this extent, the non-linear terms in 20 are expanded into a Taylor series about the reference equilibrium point ($K_1 = \phi_1 = 0$) up to the second order, so that all the relevant terms in the second derivative of the total potential energy are considered. Mathematically,

$$\frac{1}{K} = \frac{1}{K_0 + K_1} = \frac{1}{K_0} - \frac{K_1}{K_0^2} + \frac{K_1^2}{K_0^3} + O(K_1^3) \tag{28a}$$

$$\tag{28b}$$

Additionally, the coefficients d_1 and d_2 contained in Eq. 20 and expanded in Eq. 21 depend on μ, which is a non-linear function of K. Hence, the following expansion can be used:

$$\mu = \sqrt{\frac{m}{K_0}} - \frac{1}{2}\sqrt{\frac{m}{K_0^3}}K_1 + \frac{3}{8}\sqrt{\frac{m}{K_0}}K_1^2 = $$
$$= \mu_0 + \mu_1 K_1 + \mu_2 K_1^2 \tag{29}$$

13

where $m = \sqrt{\dfrac{2t}{\sqrt{12(1-\nu^2)}}}$

Substituting this result in Eq. 21, the coefficients d_1 and d_2 can be expanded in the following polynomial forms:

$$d_1 = d_{10} + d_{11}K_1 + d_{12}K_1^2 \tag{30a}$$

$$d_2 = d_{20} + d_{21}K_1 + d_{22}K_1^2 \tag{30b}$$

where the expressions of the constants $d_{ij}, i \in [0,1], j \in [0,1,2]$ are omitted here due to their length, but can be easily computed with standard symbolic solvers.

Finally, substituting Eqs. 28 and 30 in Eq. 20, the following expressions for the global forces in the adjacent equilibrium configuration are obtained:

$$
M = -Db\left\{ \left(d_{10} + d_{11}K_1 + d_{12}K_1^2\right)\left[\phi_1^2\left(\frac{3K_1^2}{K_0^4} - \frac{2K_1}{K_0^3} + \frac{1}{K_0^2}\right) - \nu\right]\left[\phi_1^2\left(\frac{K_1^2}{K_0^3} - \frac{K_1}{K_0^2} + \frac{1}{K_0}\right) + \nu(K_0 + K_1) \pm \frac{1}{r}\right] \right.
$$
$$
\left. + \left(\frac{K_1^2}{K_0^3} - \frac{K_1}{K_0^2} + \frac{1}{K_0}\right)\left(d20 + d21K_1 + d22K_1^2\right)\left[\phi_1^2\left(\frac{K_1^2}{K_0^3} - \frac{K_1}{K_0^2} + \frac{1}{K_0}\right) + \nu(K_0 + K_1) \pm \frac{1}{r}\right]^2 - \left(1 - \nu^2\right)(K_0 + K_1) \right\}
\tag{31a}
$$

$$
T = 2Db\left\{ \phi_1\left(d_{10} + d_{11}K_1 + d_{12}K_1^2\right)\left[\nu\phi_1^2\left(\frac{3K_1^2}{K_0^4} - \frac{2K_1}{K_0^3} + \frac{1}{K_0^2}\right) \pm \frac{1}{r}\left(\frac{K_1^2}{K_0^3} - \frac{K_1}{K_0^2} + \frac{1}{K_0}\right)\right] + (1 - \nu)\phi_1 \right\}
\tag{31b}
$$

These equations can be conveniently written as the sum of the equilibrium value and the variation due to the perturbations K_1 and ϕ_1. The global bending moment would become $M = M_0 + M_1$, where $M_0 = M|_{K_1=0,\phi_1=0}$ and $M_1 = M - M_0$. For the twisting moment, the equilibrium value is zero because there is no initial twist and the tape spring is isotropic, so the only contribution is given by the perturbation, i.e. $T = T_1$.

Substituting these expression into Eq. 23, the following components of the 2×2 tangent stiffness matrix are obtained:

$$
C_{11} = \left.\frac{\partial^2 \delta\Pi}{\partial \bar{K}_1^2}\right|_{\bar{K}_1=0,\bar{\phi}_1=0} = \int_0^L \left[\frac{\partial^2}{\partial \bar{K}_1^2}(M_0 + M_1)(K_0 + K_1) + T_1\phi_1\right]dx =
$$
$$
= -\frac{2Db}{r}\left\{\frac{d_{22}}{r}(1 - rK_0\nu)^2 + (d_{11} - 2d_{21} + d_{10}K_0)\nu - r\left[(1 - \nu^2) + (d_{10} - d_{20} + 2(d_{11} - d_{21})K_0 + d_{12}K_0^2)\nu^2\right]\right\}
$$
$$
\left(\frac{2\pi n}{L}\right)^4 \int_0^L \cos^4\left(\frac{2\pi nx}{L}\right)dx =
$$
$$
= -\frac{DLb}{r}\left(\frac{2\pi n}{L}\right)^4\left\{\frac{d_{22}}{r}(1 - rK_0\nu)^2 + (d_{11} - 2d_{21} + d_{10}K_0)\nu - r\left[(1 - \nu^2) + (d_{10} - d_{20} + 2(d_{11} - d_{21})K_0 + d_{12}K_0^2)\nu^2\right]\right\}
\tag{32a}
$$

$$
C_{12} = C_{21} = \left.\frac{\partial^2 \delta\Pi}{\partial \bar{K}_1 \partial \bar{\phi}_1}\right|_{\bar{K}_1=0,\bar{\phi}_1=0} = 0 \tag{32b}
$$

$$
C_{22} = \left.\frac{\partial^2 \delta\Pi}{\partial \bar{\phi}_1^2}\right|_{\bar{K}_1=0,\bar{\phi}_1=0} = -\frac{DLb}{rK_0}\left(\frac{2\pi n}{L}\right)^2\left\{d_{10} - 2\left[rK_0(1-\nu) + d_{20}(1 - \nu rK_0)\right]\right\} \tag{32c}
$$

The first interesting observation is that, starting from a twist-free equilibrium configuration, the stiffness matrix is diagonal, so bending and twisting are decoupled. As a consequence, the bending and torsional stiffness are the eigenvalues of the matrix, hence the stability boundary is reached when either the bending (C_{11}) or the torsional stiffness (C_{22}) become negative.

Since the integral of the mode shape is always positive, the sign of the stiffness does not depend on the perturbation considered, which only affects the numerical value of the stiffness and the change of energy associated to the deformation. This observation agrees with the findings from the numerical model previously discussed, and provides a physical justification for its results.

14

Hence, the stability boundary only depends on the geometry of the cross-section and the material properties of the tape spring. The plots in Figs. 14, 15 and 16 show the critical ratio R/r for which the tape spring becomes unstable as a function of the angle subtended by the cross-section, the thickness of the shell and the Young's modulus, respectively.
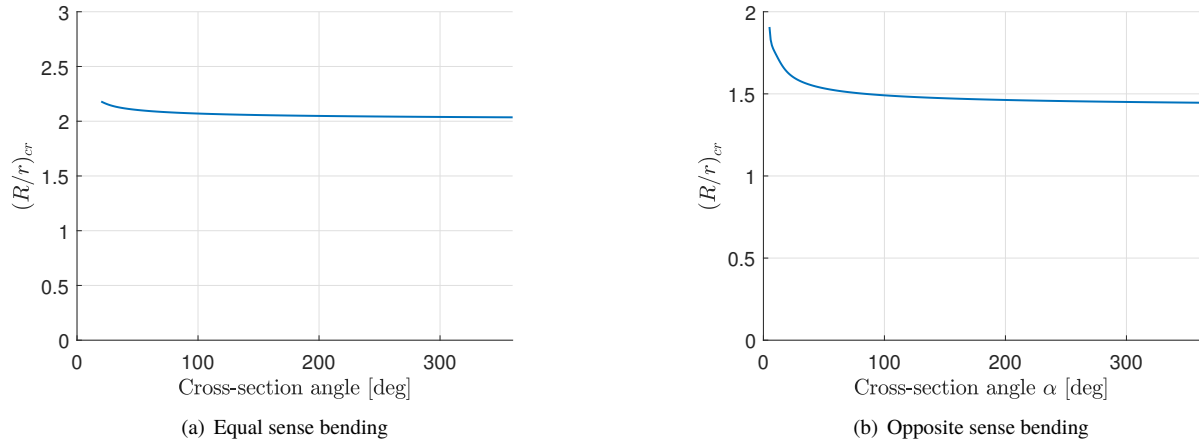

(a) Equal sense bending

(b) Opposite sense bending

Fig. 14   Stability boundary for coiled tape springs as a function of the angle subtended by the cross-section, assumed of fixed width

(a) Equal sense bending

(b) Opposite sense bending
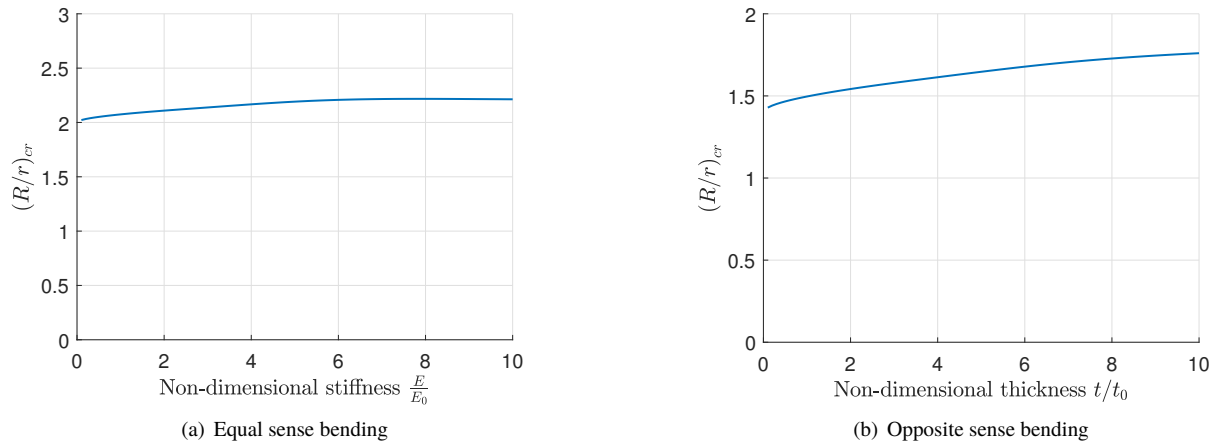
Fig. 15   Stability boundary for coiled tape springs as a function of non-dimensional shell thickness (reference value $t_0 = 0.1$ mm)

The comparison between these results and the parametric study in Sec. IV shows limited agreement on the prediction of the stability boundary both for equal and opposite sense coiling. From the analytical model, the critical ratio R/r is expected to decrease with the angle α subtended by the cross-section, apparently converging to an horizontal asymptote for large angles, whereas FEM predicts a linear growth. As for the shell thickness, the analytical model shows an increase in the stability limit when increasing the thickness, but does not capture the cubic variation of R/r observed from FEM. Finally, both the analytical and numerical models agree on the fact that the Young's modulus of the tape spring does not impact the stability limit.

In conclusion, the analytical study developed in this section does not accurately predict the stability boundary for coiled tape springs and requires further investigation. A possible reason for the disagreement is having neglected the dependence of the cross-sectional shape w on the longitudinal coordinate x, which allowed to obtain an analytical solution to the governing equation (Eq. 9).

(a) Equal sense bending   (b) Opposite sense bending
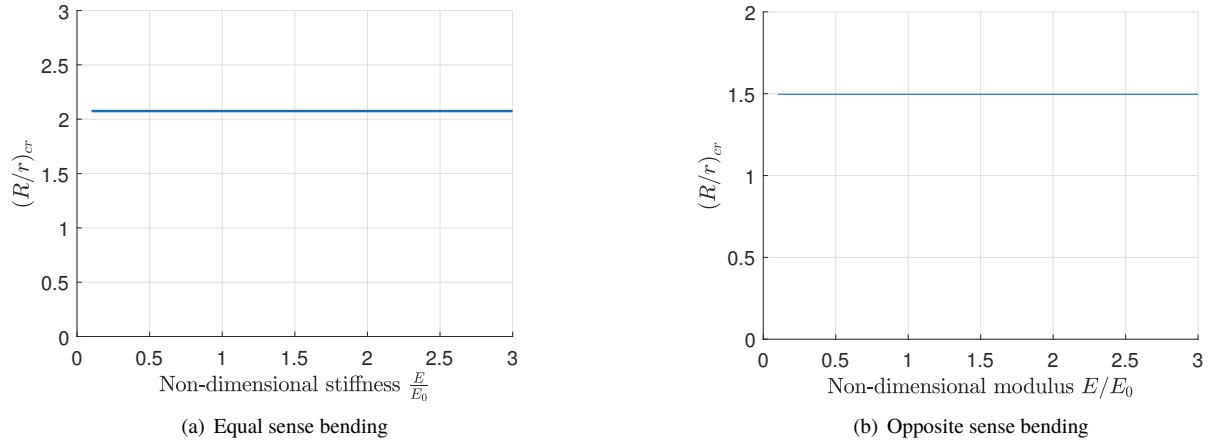
Fig. 16   Stability boundary for coiled tape springs as a function of the non-dimensional Young's modulus (reference value $E_0 = 210$ GPa)

VI. Effects of Finite Length and Contact Conditions

The previous sections have explored the stability behavior of coiled isotropic tape springs by using an idealized model, which allowed for a simplified analytical formulation and more efficient numerical simulations. The parametric study in Sec. IV provided a useful design tool for deployable structures based on tape spring-like isotropic booms and their deployment systems. However, the simplified model considered so far is based on two strong assumptions:

- the boom is infinitely long, hence edge effects can be neglected, and
- no relative motion occurs between adjacent coils, so they all behave as a single loop.

In this section, the validity of these hypotheses will be examined by relaxing them and analyzing their effects on the stability of the coiled tape spring. This will provide useful insight about the range of applicability of the previously obtained results and a better understanding of secondary effects.

A. Description of the Model

The finite element model developed for this study consists of a quasi-static implicit step, in which an initially straight tape spring is coiled around a rigid cylindrical hub of radius R. The cross-section and material of the tape spring were fixed, whereas different lengths were considered to obtain one or multiple loops in the coiled configuration.
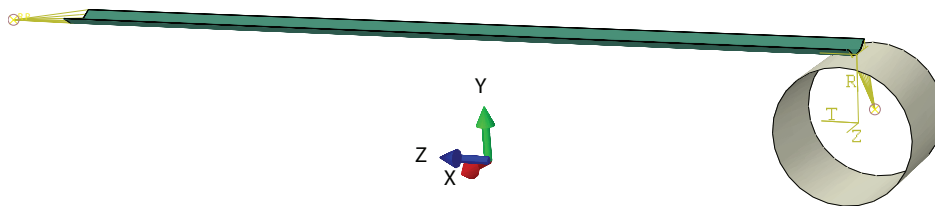
Fig. 17   Initial geometry used for the finite element model simulating the multi-loop coiling process.

The boundary conditions were chosen such that the ends of the tape spring were allowed to change their cross-sectional shape. In particular, one of the ends was connected to the axis of the hub using coupling constraint, so that tangential displacements and rotations about the hub axis were constrained, but displacements and rotations in the plane containing the cross-section were not. This allowed control of the coiling process by assigning the angular velocity of the hub about its axis, which in turn pulled the tape spring and forced its coiling.

The other end of the tape spring was connected to a reference point which only constrained axial displacements and torsion of the cross-section, but not displacements in its plane. The length of the tape spring was chosen such that a small portion of the boom remained straight at the end of the packaging, in order to reduce the influence of the boundary condition on the overall stability behavior.

16

The objective of this step was to obtain an uniformly coiled configuration to use as reference for a stability analysis. Therefore, it was necessary to suppress undesired unstable modes that could result in non-uniform final configurations and significantly increase the computational cost of the simulation.

In particular, out-of-plane instabilities were sometimes observed during the coiling of long booms, due to torsional oscillations of the region to be coiled or slipping between adjacent loops in the coiled region. To suppress them, out-of-plane displacements and torsional rotations of the midline were prevented, effectively enforcing symmetry about the X-axis.

Additionally, when the ratio R/r is sufficiently large, periodic buckles formed in the coiled region. To prevent them, a 5 N tensile force was applied to the reference point at the tip of the tape spring. The magnitude of the force was chosen as the smallest value for which no buckles could be observed.

Self-contact on the tape spring was also included, to account for the variation of the coiled radius with the number of loops.

At the end of the coiling step, the hub and the tip force were removed, while the ends of the coiled tape spring were clamped to prevent self-deployment. The resulting model was used as a starting point for a modal analysis meant to assess the stability of the equilibrium configuration by checking the sign of the smallest eigenvalue.

B. Effect of Number of Loops

The first question addressed by this model was to understand how the eigenvalues and the stability boundary were affected by the number of loops of the coiled boom.

An aspect that is worth mentioning is the way contact conditions are treated in the frequency step. Whenever it is preceded by a non-linear analysis, the system is actually linearized about the final configuration at the end of the previous step. The calculation of the mode shapes does not consider new possible contacts because the displacements are normalized, but nodes already in contact are not allowed to separate.

Therefore, in the equilibrium step run at the end of the coiling process, the midline of the tape spring was clamped so that the loops were kept in contact. During the following frequency step, the degrees of freedom of the inner loops were suppressed, effectively satisfying the hypothesis that all the loops were undergoing the same deformation modes. Consequently, the unstable mode shapes obtained by this model are qualitatively the same as those found with the idealized model, as shown in Fig. 18.


(a) Mode 1	(b) Mode 2	(c) Mode 3
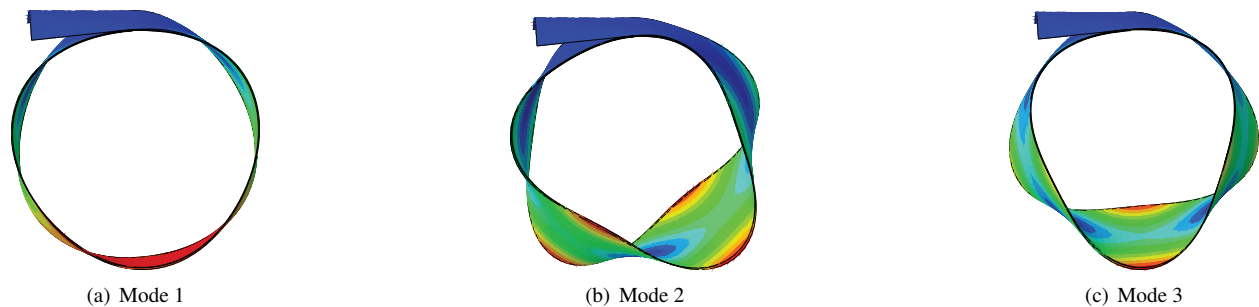
Fig. 18   First 3 unstable modes for a coiled tape springs with 3 loops and ratio $R/r = 1.5$. In this model, all the loops are bonded together and have the same mode shape.

In figure 19 the lowest eigenvalues for equal and opposite sense coiling are plotted for different number of loops. The results obtained from the idealized model have been added for comparison.

These results show a significant deviation from the infinite length approximation, which seems to overpredict the stability of equal sense-coiled tape springs and underpredict the case of opposite sense coiling. However, varying the number of coils does not affect the stability limit.

A possible conclusion that could be drawn from these results is that, as expected, the boundary conditions play a significant role on the stability of coiled tape springs and affect the global dynamics even if limited to a small region. Therefore, when designing a deployable boom for engineering applications, an accurate representation of the actual boundary conditions provided by the deployment mechanism is essential for obtaining reliable estimates.

On the other hand, the number of coils is not a determining factor for identifying the stability boundary of a tape spring, suggesting that even a single coil is sufficient to capture this behavior. This is advantageous for computational
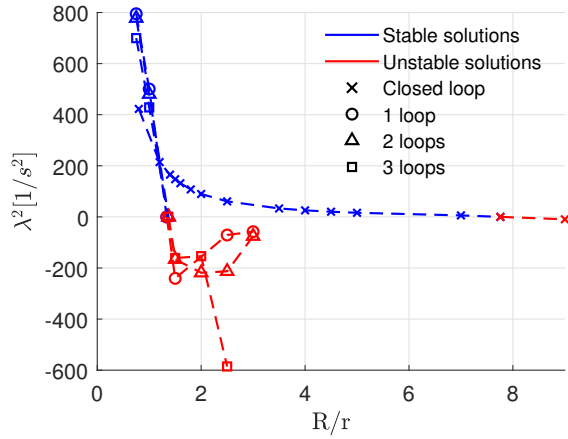
(a) Equal sense coiling
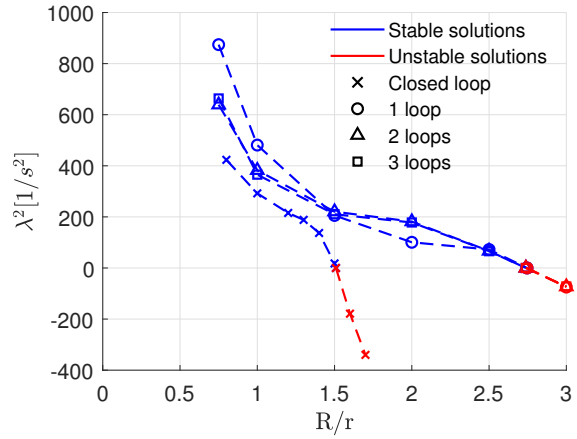
(b) Opposite sense coiling

Fig. 19 **First eigenmode of a coiled tape spring as a function of the ratio R/r, for a the infinite length case and for variable number of loops. Blue lines correspond to stable configurations, red lines to the unstable regime.**

efficiency.

C. Effect of Relative Sliding between Loops

One of the main hypotheses used throughout this study was that all the loops of the coiled tape spring behave in the same way, thus allowing the analysis of a representative element. In this section, this hypothesis will be abandoned and its consequences will be explored.

While the coiling step described in Sec. VI.A was unchanged, the contact between adjacent loops was removed in the equilibrium step. Also, the midline was clamped during the equilibrium phase, to prevent instabilities from appearing before the frequency step. After achieving equilibrium, the constraint on the midline was removed and a modal analysis was completed to determine the stability of the coiled tape spring. As a result of this modification, the stability analysis was run on a model where the loops were independent of each other.


(a) Equal sense coiling (b) Opposite sense coiling
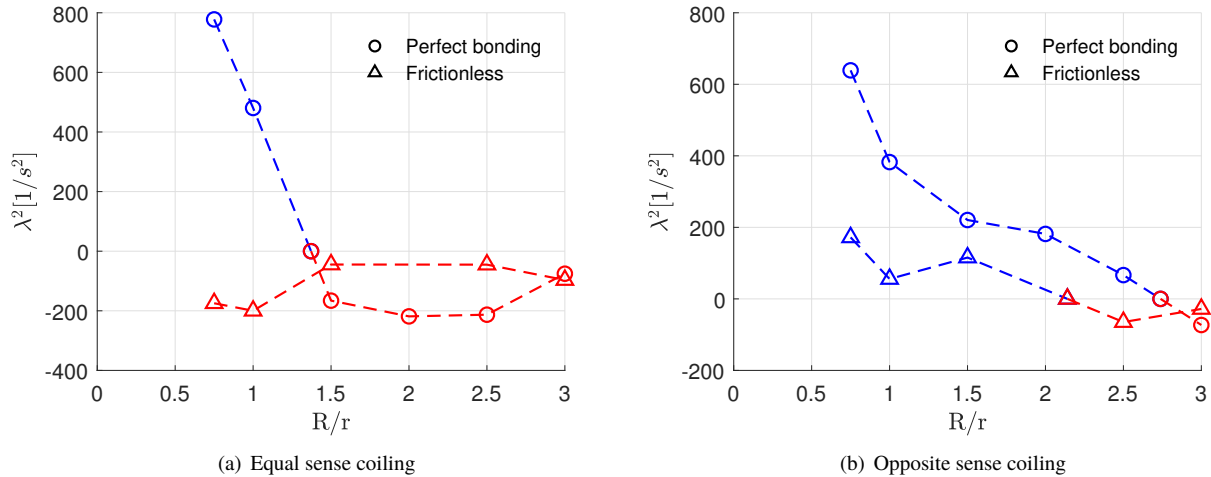
Fig. 20   First eigenmode of a coiled tape spring as a function of the ratio R/r, for different contact conditions. Perfect bonding refers to the case in which no relative motion between adjacent coils is allowed; frictionless contact considers the coils independent of each other. The results are derived for 2-loop coiling. Blue lines correspond to stable configurations, red lines to the unstable regime.

Fig. 20 show the evolution of the eigenvalues predicted by the frictionless model and compares it with the results from Sec. VI.B. The results refer to 2-loop coils since this is the smallest number of loops for which self-contact conditions can be studied. The main result from this study is that the onset of the instability occurs for lower ratios R/r and, in equal sense coiling, no stable region exists.

From the analysis of the mode shapes, the most noticeable observation is the existence of new instability modes occurring at any ratio R/r. In particular, equal-sense coiled tape springs are characterized by torsional instabilities, in which the inner coil rotates with respect to the outer coil as if they were hinged together. Fig. 21 shows a sequence of the development of this instability mode, computed with a dynamic implicit analysis, in which frictionless self-contact is formulated.

In opposite sense coiling, the mode shape described in Fig. 21 was observed too, but it was always stable. However, for ratios $R/r > 2$, the deformation mode responsible for the onset of the instability was found to be a blossoming mode, in which the inner coil reduces its radius of curvature trying to reach its natural radius, i.e. $R/r = 1$. This instability is responsible for a reduction of the critical ratio from $R/r = 2.7$ as predicted by the closed loop model to $R/r = 2.2$.

It is worth noting that two sets of lines shown in Fig. 20 set an upper and lower bound to the stability limit of real tape springs, where self-contact is characterized by a finite value of the friction coefficient. Therefore, in the design process of stably-coiled tape springs, tuning the friction properties or using weak adhesives between adjacent coils could widen the stable design space and approach the perfect bonding limit.
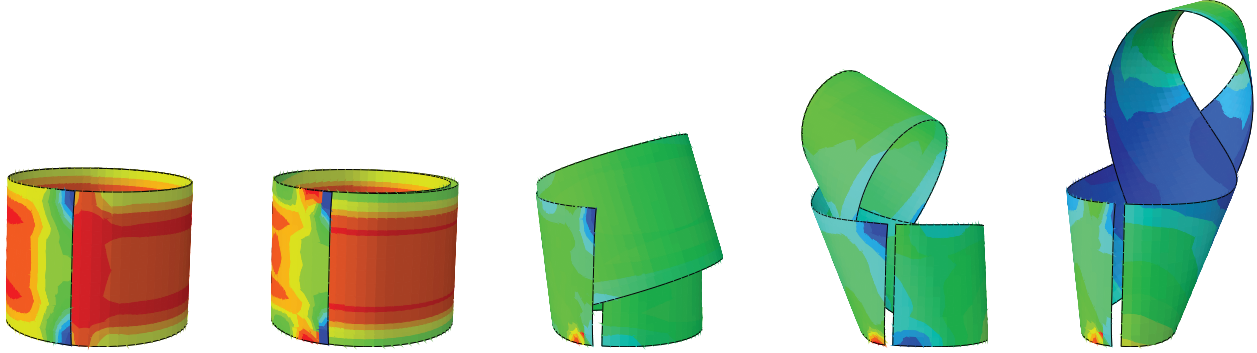
Fig. 21   Evolution of out-of-plane instabilities for a coiled tape spring without friction, for the case $R/r = 1$ and 2 loops. Colors show Von Mises stress distribution.

VII. Conclusion

This paper has proposed a computational framework to study the stability of coiled tape springs in the absence of tension-stabilization. The numerical results suggest that non-uniform deformation modes drive the stability of tape springs and that there exists a limited range of R/r values for which the equilibrium is stable. Two dominant unstable modes were identified, depending on the coiling direction. For opposite sense coiling, the instability is triggered by torsional modes, whereas bending modes are responsible for the instability of equal-sense coiled tape springs.

A parametric study was conducted to understand the effect of the geometry and material of isotropic tape springs on the critical value R/r and derive stability boundaries in the design space.

An analytical solution was also developed to predict non-uniform torsional and bending modes. The model showed that in the uniformly coiled configuration bending and torsion are decoupled, and hence the instability is driven by the bending or torsional stiffnesses becoming negative. The instability is independent from the wavenumber of the mode shape. However, the stability limits obtained from the numerical and analytical solutions developed in this paper do not fully agree, and further investigation of the problem will be needed to establish .

Edge effects on the stability of finite length coiled tape springs were also studied numerically, leading to the conclusion that the boundary conditions have a significant impact on the stability behavior. This suggests a possible direction for future research, in which the interaction between deployment mechanisms and deployable booms could be investigated, by considering different boundary conditions and their impact on the stability of the system.

On the other hand, we did not observe any dependency of the critical ratio R/r on the number of coils. This suggests that studying the stability of relatively long booms can be simplified by only considering a portion of them. Lastly, the effect of allowing relative motion between adjacent coils was studied. In the limit case of negligible self-contact, the existence of out-of-plane instability modes was observed on equal-sense coiled tape spring, that resulted in unstable behaviors for any ratio of R/r. For opposite-sense coiled tape springs, allowing relative motion reduced the stability limit because of the appearance of blossoming deformation modes.

The analysis framework developed in this work could help the design of intrinsically stable deployable structures that require limited constraints in the stowed configuration. Although it was developed for isotropic tape springs, it could be easily extended to more general boom cross-sections and composite materials.

Acknowledgments

References

[1] Galletly, D. A., and Guest, S. D., "Bistable composite slit tubes. I. A beam model," *International Journal of Solids and Structures*, Vol. 41, No. 16-17, 2004, pp. 4517–4533.

[2] Galletly, D. A., and Guest, S. D., "Bistable composite slit tubes. II. A shell model," *International Journal of Solids and Structures*, Vol. 41, No. 16-17, 2004, pp. 4503–4516.

[3] Iqbal, K., and Pellegrino, S., "Bi-stable composite shells," *41st Structures, Structural Dynamics, and Materials Conference and Exhibit*, 2000, p. 1385.

[4] Leclerc, C., Pedivellano, A., and Pellegrino, S., "Stress Concentration and Material Failure During Coiling of Ultra-Thin TRAC Booms," *2018 AIAA Spacecraft Structures Conference*, 2018, p. 0690.

[5] Leclerc, C., Wilson, L. L., Bessa, M. A., and Pellegrino, S., "Characterization of Ultra-Thin Composite Triangular Rollable and Collapsible Booms," *4th AIAA Spacecraft Structures Conference*, 2017, p. 0172.

[6] Murphey, T., Jeon, S., Biskner, A., and Sanford, G., "Deployable booms and antennas using bi-stable tape-springs," 2010.

[7] Heidt, H., Puig-Suari, J., Moore, A., Nakasuka, S., and Twiggs, R., "CubeSat: A new generation of picosatellite for education and industry low-cost space experimentation," 2000.

[8] Costantine, J., Tawk, Y., Christodoulou, C. G., Banik, J., and Lane, S., "CubeSat deployable antenna using bistable composite tape-springs," *IEEE Antennas and Wireless Propagation Letters*, Vol. 11, 2012, pp. 285–288.

[9] Calladine, C., "The theory of thin shell structures 1888–1988," *Proceedings of the Institution of Mechanical Engineers, Part A: Power and Process Engineering*, Vol. 202, No. 3, 1988, pp. 141–149.

[10] Lappas, V., Adeli, N., Visagie, L., Fernandez, J., Theodorou, T., Steyn, W., and Perren, M., "CubeSail: A low cost CubeSat based solar sail demonstration mission," *Advances in Space Research*, Vol. 48, No. 11, 2011, pp. 1890–1901.

[11] Wilson, L., Gdoutos, E. E., and Pellegrino, S., "Tension-Stabilized Coiling of Isotropic Tape Springs," , 2018. Submitted.

[12] Hoskin, A., Viquerat, A., and Aglietti, G. S., "Tip force during blossoming of coiled deployable booms," *International Journal of Solids and Structures*, Vol. 118, 2017, pp. 58–69.

[13] Seffen, K., and Pellegrino, S., "Deployment dynamics of tape springs," *Proceedings of the Royal Society of London A: Mathematical, Physical and Engineering Sciences*, Vol. 455, The Royal Society, 1999, pp. 1003–1048.

[14] Galletly, D. A., and Guest, S. D., "Equilibrium and stability analysis of composite slit tubes," *Proceedings of the IASS-IACM*, 2000.

[15] Guest, S., and Pellegrino, S., "Analytical models for bistable cylindrical shells," *Proceedings of the Royal Society of London A: Mathematical, Physical and Engineering Sciences*, Vol. 462, The Royal Society, 2006, pp. 839–854.

[16] Ilanko, S., Monterrubio, L., and Mochida, Y., *The Rayleigh-Ritz method for structural analysis*, John Wiley & Sons, 2015.

[17] Brush, D. O., and Almroth, B. O., *Buckling of bars, plates, and shells*, Vol. 6, McGraw-Hill New York, 1975.

[18] *Abaqus Documentation*, 2016.

[19] Calladine, C. R., *Theory of Shell Structures*, Cambridge University Press, 1983. doi:10.1017/CBO9780511624278.